Wave propagation in one-dimensional fluid-saturated porous metamaterials

Yan-Feng Wang,[1,2] Jun-Wei Liang,[2] A-Li Chen,[2] Yue-Sheng Wang,[1,*] and Vincent Laude[3,†]
[1]*School of Mechanical Engineering, Tianjin University, 300350 Tianjin, China*
[2]*Institute of Engineering Mechanics, Beijing Jiaotong University, 100044 Beijing, China*
[3]*Institut FEMTO-ST, Université Bourgogne Franche-Comté, CNRS, 25030 Besançon, France*

(Received 21 December 2018; revised manuscript received 14 March 2019; published 16 April 2019)

Fluid-saturated porous metamaterials described following Biot's theory support two longitudinal elastic waves. The phase velocity and attenuation of these waves depend nonlinearly on porosity and viscosity of the fluid. Furthermore, when two fluid-saturated porous metamaterials are arranged to form a periodic composite, different band gaps are opened for the two longitudinal waves and these couple to form anticrossings in the dispersion relation. The complex band structure of one-dimensional composites is derived and compared with numerical transmission through a finite sample obtained by the finite element method. It is found that the anticrossings disappear rapidly as viscosity increases, while attenuation band gaps become dominated by the fastest of the two longitudinal waves. Increasing porosity further leads to wider and lower-frequency band gaps. These results are relevant to practical applications of fluid-saturated porous metamaterials, e.g., to engineered soils.

DOI: 10.1103/PhysRevB.99.134304

I. INTRODUCTION

Wave propagation in geological materials or ground [1] has received considerable attention because of its practical importance in various fields such as earthquake engineering, soil dynamics, geophysics, hydrology, etc. Most existing studies deal with ground vibrations caused by mechanical operation or seismic waves [2]. A great deal of research has already been conducted on constructing wave barriers operating between the vibration source and the protected structures [3]. More recently, periodic wave barriers, inspired by the concept of phononic crystals (PCs), have attracted more and more attention [4]. PCs are spatially periodic composites composed of different materials [5]. They can exhibit frequency band gaps in their transmission spectrum, where the propagation of acoustic or elastic waves is fully prohibited. The PC concept was proposed in 1993, although there had been many works about wave propagation in periodic media and structures before [6]. In 2000, Liu *et al.* [7] further introduced the concept of local resonance inducing complete band gaps at low frequencies and providing a negative dynamic effective-mass density inside resonant band gaps [8]. Locally resonant PCs are also termed acoustic or elastic metamaterials [9], since their band gaps are not significantly dependent on periodicity. PCs and metamaterials provide new ways to manipulate acoustic and elastic waves. The ambition of *band-gap engineering* [10] is to control wave propagation.

A direct application of band-gap engineering is noise isolation and vibration reduction. Niousha and Motosaka [4] investigated the effects of periodic wave barriers on the reduction of ground vibration. Jia and Shi [11] studied the influence of physical and geometrical parameters of periodic foundation on the band gaps. Malcolm and Nicholls [12] examined the scattering of periodic multilayered media. Bao *et al.* [13] discussed the dynamic response of a seven-storey frame structure with periodic foundations. Kim and Das [14] proposed an earthquake-resistant design by constructing a shell-type waveguide composed of many Helmholtz resonators. Shi and Huang [15] described the feasibility of reducing seismic waves by locally resonant metamaterials. Mitchell *et al.* [16] proposed a metaconcrete composed of designed aggregates to enhance dynamic performance. Colombi *et al.* [17] designed a seismic metawedge to convert destructive Rayleigh seismic waves into harmless bulk shear waves. Colquitt *et al.* [18] carefully analyzed the canonical problem of an array of subwavelength resonators placed on either a thin elastic plate or an elastic half-space. On the experimental side, a full-scale experiment aiming at researching the interaction of structured soil with seismic waves was realized by Brûlé *et al.* [19]. Yan *et al.* [20] conducted field experiments of a scaled periodic foundation. Colombi *et al.* [21] demonstrated experimentally that a Rayleigh wave experiences strong attenuation when interacting with a forest acting as a locally resonant metamaterial.

Although numerous theoretical studies have explored the properties of PCs and metamaterials, they often consider soil as an elastic constituent, within which waves furthermore often propagate without attenuation. Some studies of PCs or metamaterials composed of fluid-saturated porous (FSP) media have emphasized their specific acoustic properties [22–25] and have also discussed wave attenuation in FSP media [26]. Actually, wave propagation in FSP media has attracted significant attention for a long time [27–30]. The related theory is of great significance in the fields of geophysical exploration, seismic engineering, or geodynamics. Biot [31,32] formulated the basic equations for isotropic FSP media. It follows from

*yswang@tju.edu.cn
†vincent.laude@femto-st.fr

this theory that two longitudinal and two transverse waves exist. Plona [33] and Dutta [34] later proved this fact: the speed of the slow compressional wave is smaller than the speed of sound in the fluid. Wave propagation in FSP media has since then been investigated from different viewpoints and by using different methods [35–39]. The effect on the propagation of elastic waves of the material parameters of the fluid, the solid skeleton, and of their combination was discussed. Slowness surfaces [38] and wavefronts [40] were calculated by using plane-wave theory or characteristic analysis. We note that previous investigations of PCs involving FSP media [22–26] have not specifically considered the possible interference of the two longitudinal waves.

In this paper, we conduct a detailed analysis of the dynamical behavior of wave propagation in one-dimensional fluid-saturated porous metamaterials (FSPMs). Of particular interest is the mutual interaction of the two longitudinal acoustic waves in FSP media and how they attenuate differently in FSPMs. The basic equations are first summarized in Sec. II. Harmonic Bloch wave propagation and its finite element implementation are discussed in Sec. III. These equations are used in Sec. IV to obtain dispersion relations. To start with, we study wave propagation in homogeneous FSP media. We then consider the effect of viscosity and porosity on the complex band structure and the frequency response function of one-dimensional FSPMs. Only normal-incidence longitudinal waves are considered in this paper. Extensions of our approach to general incidence and more periodicities are suggested in the conclusion.

II. BASIC EQUATIONS

Following Biot [31,32], the constitutive equations for wave propagation in an isotropic FSP media can be written

$$\begin{aligned}
\tau_{xx} &= (2B_1 + B_2)e_{xx} + B_2 e_{yy} + B_2 e_{zz} + B_3\xi,\\
\tau_{yy} &= B_2 e_{xx} + (2B_1 + B_2)e_{yy} + B_2 e_{zz} + B_3\xi,\\
\tau_{zz} &= B_2 e_{xx} + B_2 e_{yy} + (2B_1 + B_2)e_{zz} + B_3\xi,\\
\tau_{yz} &= 2B_1 e_{yz},\\
\tau_{zx} &= 2B_1 e_{zx},\\
\tau_{xy} &= 2B_1 e_{xy},\\
p &= B_3 e_{xx} + B_3 e_{yy} + B_3 e_{zz} + B_4\xi. \qquad (1)
\end{aligned}$$

In these expressions, τ_{ij} and e_{ij} $(i, j = x, y, z)$ are the stress and strain tensors of the solid skeleton, p is the pore fluid pressure, and ξ is the increment of the fluid content per unit volume. The displacement components of the skeleton and of the fluid are u_i and U_i. All these quantities are functions of position. The strain e_{ij} and the increment ξ can be expressed as

$$e_{ij} = \tfrac{1}{2}(u_{i,j} + u_{j,i}), \quad \xi = -w_{i,i}, \qquad (2)$$

where $w_i = \phi(U_i - u_i)$ and ϕ is the porosity of the medium (a number between 0 and 1). The notation $u_{i,j} = \frac{\partial u_i}{\partial x_j}$ is used for brevity where applicable. The material coefficients B_1 to B_4 are spatially periodic functions determined by the material properties of the solid skeleton and fluid [41]:

$$\begin{aligned}
B_1 &= C_{44}, \quad B_2 = C_{12} + B_3^2/B_4,\\
B_3 &= -\left[1 - \frac{1}{3K_s}(C_{11} + 2C_{12})\right]B_4,\\
B_4 &= \left[\frac{1-\phi}{K_s} + \frac{\phi}{K_f} - \frac{1}{3K_s^2}(C_{11} + 2C_{12})\right]^{-1},
\end{aligned}$$

where the C_{ij} are the elastic constants of the solid skeleton, and K_s and K_f are the bulk modulus of the solid skeleton and the pore fluid, respectively.

The equations of motion can be written in Cartesian coordinates as

$$\tau_{ij,j} = \rho\ddot{u}_i + \rho_f\ddot{w}_i, \quad -p_{,i} = \rho_f\ddot{u}_i + m_{ii}\ddot{w}_i + r_{ii}\dot{w}_i, \qquad (3)$$

where $\rho = (1-\phi)\rho_s + \phi\rho_f$, ρ_f, and ρ_s are the mass densities of the FSP media, the solid skeleton, and the pore fluid, respectively. m_{ii} and r_{ii} are coefficients introduced by Biot. For isotropic FSP materials, we have $m_{11} = m_{22} = m_{33} = m$ and $r_{11} = r_{22} = r_{33} = r$.

Without loss of generality, we limit our discussion to longitudinal motion restricted to the x direction. For illustration, we consider an inhomogeneous FSPM with a periodic alternation of layers, as shown in Fig. 1. Combining the above equations, we have

$$\begin{aligned}
\frac{\partial}{\partial x}\left[(2B_1 + B_2)\frac{\partial u_x}{\partial x}\right] - \frac{\partial}{\partial x}\left(B_3\frac{\partial w_x}{\partial x}\right) &= \rho\ddot{u}_x + \rho_f\ddot{w}_x,\\
-\frac{\partial}{\partial x}\left(B_3\frac{\partial u_x}{\partial x}\right) + \frac{\partial}{\partial x}\left(B_4\frac{\partial w_x}{\partial x}\right) &= \rho_f\ddot{u}_x + m\ddot{w}_x + r\dot{w}_x \qquad (4)
\end{aligned}$$

for longitudinal wave motion. Thus, the two independent variables are chosen as (u_x, w_x). If at the interface between two FSP media longitudinal displacements are considered continuous, the open pore condition, then the natural boundary condition is the continuity of both normal stresses $(2B_1 + B_2)u_{x,x} - B_3 w_{x,x}$ and $-B_3 u_{x,x} + B_4 w_{x,x}$.

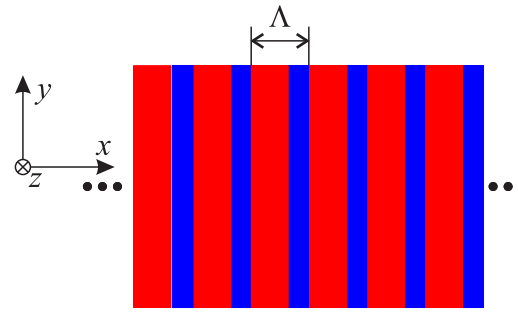

FIG. 1. Sketch of the 1D fluid-saturated porous metamaterial with a periodic alternation of two layers. The lattice constant is Λ. Periodicity is along the x direction; the other two directions are infinite.

III. HARMONIC WAVE PROPAGATION

A. Harmonic waves

For harmonic waves at angular frequency ω, longitudinal displacements can be written

$$[u_x, w_x] = [\bar{u}_x, \bar{w}_x]e^{-i\omega t}, \tag{5}$$

where t is the time variable, and where $\bar{u}_x$ and $\bar{w}_x$ are functions of position x otherwise independent of time. Here, we note $\mathbf{U} = (\bar{u}_x, \bar{w}_x)$. Substituting Eq. (5) into Eq. (4), we get

$$\frac{\partial}{\partial x}\left(A_0\frac{\partial}{\partial x}\mathbf{U}\right) = -\rho\omega^2 M_0\mathbf{U}, \tag{6}$$

with

$$A_0 = \begin{bmatrix}(2B_1 + B_2) & -B_3\\ -B_3 & B_4\end{bmatrix}, \quad M_0 = \begin{bmatrix}\rho & \rho_f\\ \rho_f & m_1\end{bmatrix},$$

and $m_1 = m + ir/\omega$.

The Biot coefficients m and r can be written as [28,36]

$$m = \mathrm{Re}[\alpha(\omega)]\rho_f/\phi, \quad r = \mathrm{Re}[\eta/K(\omega)], \tag{7}$$

where η is the viscosity of the fluid, and α and K are the dynamic tortuosity and permeability, respectively, with the relation

$$\alpha(\omega) = i\eta\phi/[K(\omega)\omega\rho_f]. \tag{8}$$

For porous media with pores of simple form, the dynamic permeability can be expressed approximately as [42]

$$K(\omega) = K(0)\left(\left[1 - \frac{4i\alpha^2(\infty)K^2(0)\omega\rho_f}{\eta d^2\phi^2}\right]^{1/2} - \frac{i\alpha(\infty)K(0)\omega\rho_f}{\eta\phi}\right)^{-1}, \tag{9}$$

where d is the characteristic length of the pores. When the pores are a set of nonintersecting tubes, we further have

$$8\alpha(\infty)K(0)/(\phi d^2) = 1. \tag{10}$$

B. Bloch waves

According to Bloch's theorem, the displacement field for propagation eigenmodes of a periodic medium is the product of a periodic function times a plane-wave term. It thus can be written

$$\mathbf{U}(x) = \mathbf{u}(x)e^{ikx}, \tag{11}$$

where $\mathbf{u} = (a_x, b_x)$, with a_x and b_x being the periodic amplitudes as a function of position, and k being the Bloch wave number whose real part can be restricted to the first Brillouin zone of the reciprocal lattice. Substituting Eq. (11) into Eq. (6), we get

$$\frac{\partial}{\partial x}\left(A_0\frac{\partial}{\partial x}\mathbf{u}\right) + 2ikA_0\frac{\partial}{\partial x}\mathbf{u} + (-k^2A_0 + \omega^2M_0)\mathbf{u} = 0 \tag{12}$$

for longitudinal wave motion.

In the present paper, numerical calculations are conducted with the finite element method. The layered system is treated as a periodic and inhomogeneous medium, whose material parameters are spatially periodic functions. The pores are chosen to be open at the interfaces, since the appearance of the P2 (slow) wave is restricted by the sealing of the pores at the interfaces [43]. The field variables (a_x, b_x) between different layers are set as continuous [44,45]. We write the coefficient form of the resulting equation, suitable for use with the partial differential equation (PDE) module of Comsol Multiphysics, for instance [46], as

$$\lambda^2A_1\mathbf{u} - \nabla\cdot(A_0 : \nabla\mathbf{u} + A_2\mathbf{u}) + A_3\nabla\mathbf{u} + A_4\mathbf{u} = 0, \tag{13}$$

where $\lambda = ik$ and the coefficient matrices are obtained from Eq. (12) as

$$A_1 = -A_0, \quad A_2 = -A_3 = \lambda A_0, \quad A_4 = -\omega^2M_0. \tag{14}$$

Since the dynamic material parameters of FSPMs are frequency dependent, complex band structures [46,47] are the first choice for the analysis. For this purpose, we set the eigenvalue as $\lambda = ik$. Complex band structures are then obtained by sweeping ω in the frequency range of interest.

In particular, if the pore fluid is lossless, i.e., $\eta = 0$, we have $m = \alpha(\infty)\rho_f/\phi$ nondispersive and $r = 0$ identically. Then $m_1 = m$ and Eqs. (6) and (12) do not involve frequency-dependent coefficients. In this case, we may solve Eq. (12) for the real band structure by choosing the eigenvalue as $\lambda = i\omega$. The coefficient matrices of Eq. (14) are in this case

$$A_1 = M_0, \quad A_2 = -A_3 = ikA_0, \quad A_4 = k^2A_0. \tag{15}$$

The real band structure is then obtained by sweeping k inside the first Brillouin zone of the one-dimensional (1D) periodic metamaterial.

C. Homogeneous fluid-saturated porous medium

For homogeneous FSP media, the amplitudes a_x and b_x are constant functions, so the partial terms in Eq. (12) vanish. Then Eq. (12) reduces to

$$(-k^2A_0 + \omega^2M_0)\mathbf{u} = 0. \tag{16}$$

Note that, strictly speaking, k here denotes the wave number of a harmonic plane wave rather than a Bloch wave number and $\mathbf{u}$ is a constant vector representing the polarization of the plane wave. As a result, the dispersion relation for longitudinal harmonic plane waves can be obtained as

$$k = \omega\sqrt{\frac{-b \pm \sqrt{b^2 - 4ac}}{2a}}, \tag{17}$$

where $a = B_3^2 - (2B_1 + B_2)B_4$, $b = 2\rho_f B_3 + \rho B_4 + (2B_1 + B_2)m_1$, and $c = \rho_f^2 - \rho m_1$. Equation (17) also suggests that there are two longitudinal waves in the porous medium, the sign + corresponding to the P1 (fast) wave and the sign − to the P2 (slow) wave. As a note, Eq. (4) could also be written with the fluid pressure p replacing displacement w_x as an independent variable [41]. In this case, exactly the same dispersion relation would be obtained, as we have checked. In this case, the eigenvectors defining the polarization would be different, although the following results would still hold.

D. Frequency response function

The frequency response function (FRF) [48] of a finite system can also be calculated by solving Eq. (6), in order

TABLE I. Material parameters used in this paper. Units are given inside brackets.

Material	ρ_s (kg/m^3)	ρ_f (kg/m^3)	C_{11} (GPa)	C_{12} (GPa)	C_{44} (GPa)	K_s (GPa)	K_f (GPa)	η (Pa s)	d (μm)	$\alpha(\infty)$	ϕ
Lossy FSP medium 1	3000	1000	10	2	4	30	2	0.001	6.32	1	0.2
Lossless FSP medium 1	3000	1000	10	2	4	30	2	0	6.32	1	0.2
Lossless FSP medium 2	2500	0.1	33.3	8.3	12.5	49.9	2	0	6.32	1	0.01

to compare with phononic band structures. The only nonzero coefficient matrices are in this case A_0 and $A_4 = -\omega^2 M_0$. Harmonic excitation with unit amplitude is applied to the left side of the finite system. Polarizations $(u_x, w_x) = (1, 0)$ or (0,1) are considered as excitations. Harmonic responses are measured at the right side of the system, and the frequency response function is defined as

$$\mathrm{FRF} = -\log_{10}\frac{\sqrt{\bar{u}_x^2 + \bar{w}_x^2}}{\sqrt{\bar{u}_{x0}^2 + \bar{w}_{x0}^2}}. \tag{18}$$

The imaginary part of the wave number characterizes the spatial decay of Bloch waves inside a PC [47,49]. As a result, the FRF can be approximated by using only the least evanescent Bloch wave [50]

$$\mathrm{FRF} \approx -\log_{10}(T_0 e^{-n|\mathrm{Im}(k(\omega)|\Lambda}), \tag{19}$$

where n is the number of layers, and T_0 is the conversion efficiency from the incident wave to the least evanescent Bloch wave.

IV. RESULTS AND DISCUSSION

In this section, Bloch wave propagation in a 1D FSPM is investigated, including complex band structures and harmonic responses. To get a convergent result, the size of the mesh is 100 times smaller than the lattice constant in the calculation of complex band structures, and 50 times smaller in the calculation of attenuation properties. Results for the homogeneous FSP media are first presented for reference and comparison.

A. Homogeneous fluid-saturated porous media

We first consider the case of a homogeneous FSP medium. The material parameters are listed in the second row of Table I. It should be pointed out that the tortuosity is rigorously related to the electrical conductivity of the pore space [51]. We choose the ideal case $\alpha(\infty) = 1$ for qualitative analysis [42,45]. The complex band structure $k(\omega)$ is shown in Fig. 2. It consists of two parts, showing the variations of frequency, $\omega/(2\pi)$, as a function of the real [Re(k)] and of the imaginary [Im(k)] parts of the wave number in the direction of propagation. The color scale amounts for the relative energy ratio between the kinetic energy E_k^f for the pore fluid and the kinetic energy E_k^s for the solid skeleton, defined as

$$\frac{\int e_k^s dL}{\int \left(e_k^s + e_k^f\right) dL}, \tag{20}$$

where L is the integration line along the unit cell, $e_k^s = (1-\phi)\rho_s\omega^2 u_x^2/2$ and $e_k^f = \phi\rho_f\omega^2 U_x^2/2$. Both longitudinal waves are dispersive and lossy, as a result of the viscosity of the pore fluid. The polarization of the P1 wave is mainly u_x while the polarization of the P2 wave is mostly U_x. The imaginary part of the wave number generally increases with frequency, but its value for the P2 wave is much larger than that for the P1 wave, implying a much larger attenuation. The analytical result of Eq. (17) is in excellent agreement with the finite element result.

For comparison, the band structure for the lossless homogeneous FSP medium (third row of Table I) is also plotted in Fig. 2. Im(k) is zero in this case for both waves, but Re(k) is almost unchanged for the P1 wave while it changes drastically for the P2 wave. In the low-frequency range, the imaginary and the real parts of the wave number are nearly equal in the lossy case, in agreement with the results in Ref. [45]. We correspondingly evaluate in Fig. 3 the variation of phase velocity, $\omega/\mathrm{Re}(k)$, and of the attenuation, $\log_{10}(1/Q)$, as a function of frequency. The quality factor is here defined as

$$Q = \frac{\mathrm{Re}(k)}{2\mathrm{Im}(k)}. \tag{21}$$

As a note, this definition is slightly different from that used in Ref. [28]. Three different values of viscosity are considered in Fig. 3, $\eta = 10^{-7}$, 10^{-4}, and 10^{-3} Pa s. The phase velocity of the P1 wave is not strongly affected by the value of viscosity and remains only slightly dispersive. The attenuation has larger variations with frequency: it first increases, reaches a maximum, and then decreases. The frequency of

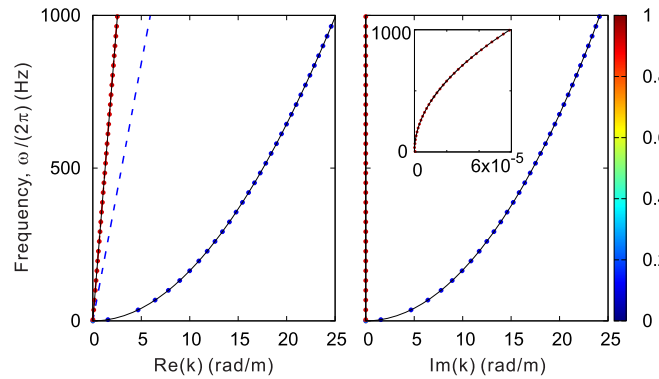

FIG. 2. Complex band structures for homogeneous FSP media. The left and right panels illustrate the variation of the frequency with the real and imaginary part of the wave vector, respectively. The solid lines represent for the analytical results obtained by Eq. (17). The color scale indicates the relative energy ratio between the solid skeleton (1) and the pore fluid (0). The blue and red dashed lines represent the analytical dispersion curves for lossless homogeneous media. The inset shows a closer view of the imaginary part at the origin.

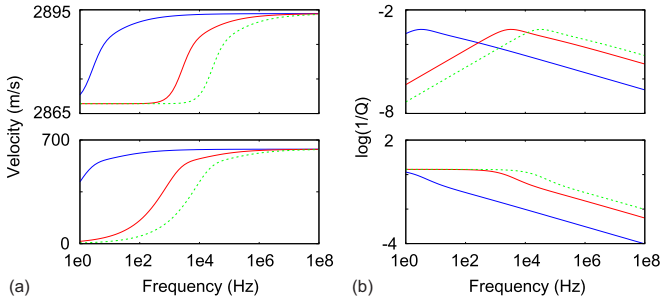

FIG. 3. Variation of (a) the phase velocity and (b) the attenuation with frequency for different viscosities of the pore fluid. The horizontal axis is shown with a logarithmic scale. The thick-solid blue, thin-solid red, and thin-dashed green lines represent the results for $\eta = 10^{-7}$, 10^{-4}, and 10^{-3} Pa s, respectively. The upper and lower panels present the results for P1 and P2 waves, respectively.

the maximum is termed the critical frequency and can be expressed as [52]

$$f_c = 3\eta\phi/[8\pi K(0)\alpha(\infty)\rho_f]. \tag{22}$$

It is thus linearly proportional to viscosity. For the chosen values of viscosity, the critical frequency is 2.4 Hz, 2.4 kHz, and 24 kHz, respectively. The phase velocity of the P2 wave, in sharp contrast, is strongly dependent on viscosity and strongly dispersive, with a sharp variation around the critical frequency. The attenuation remains almost constant until f_c and then decreases with increasing frequency. For the same value of viscosity, the attenuation of the P2 wave is generally larger than that of the P1 wave.

It is furthermore instructive to consider the dependence of the complex dispersion with porosity in Fig. 4. To enable a fair comparison, the pore size d is considered fixed. The change in porosity ϕ can then be understood as a change in the number of pores. According to Eq. (10), the critical frequency in Eq. (22) can be rewritten as

$$f_c = 3\eta/(\pi d^2\rho_f). \tag{23}$$

This expression implies that f_c is independent of porosity for a fixed pore size. It is found that porosity has a strong influence on both the phase velocity and the attenuation of the

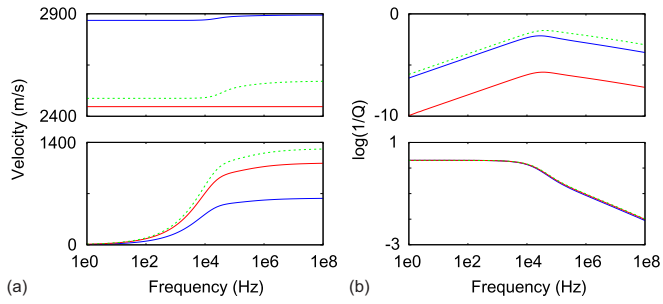

FIG. 4. Variation of (a) the phase velocity and (b) the attenuation with frequency for different values of porosity. The horizontal axis is shown with a logarithmic scale. The thick-solid blue, thin-solid red, and thin-dashed green lines present the results for $\phi = 0.05$, 0.24, and 0.45, respectively. The upper and lower panels present the results for P1 and P2 waves, respectively.

P1 wave. For the particular value $\phi = 0.24$, the phase velocity is observed to be nondispersive. This effect is contained in the FSP model summarized in Sec. II, which is based on the literature, but has not yet been observed experimentally to the best of our knowledge. At a given frequency, the phase velocity and the attenuation first decrease and then increase with increasing porosity. The attenuation of the P2 wave is almost independent of porosity, but the asymptotic value of the phase velocity at large frequencies generally increases with porosity.

B. One-dimensional lossless fluid-saturated porous metamaterial

We now turn our attention to wave propagation in 1D FSPM composed of periodic layers of FSP media. We first consider a lossless FSPM (zero viscosity). The filling ratio for FSP medium 2 is chosen to be 0.35 and the lattice constant is $\Lambda = 2$ m. Material parameters are listed in the fourth row of Table I.

The complex band structure in Figs. 5(a) and 5(b) shows reduced frequency $\Omega = \omega\Lambda/(2\pi)$ as a function of reduced wave number $k\Lambda/(2\pi)$, as usual with PCs. We consider the reduced frequency range $0 < \Omega < 2000$ m/s and the corresponding frequency range is 0–1000 Hz for the chosen lattice constant. Given the color scale representing the energy ratio between the P1 and the P2 wave, it is inferred that both longitudinal waves exist in the composite metamaterial and can form Bragg band gaps opening at the edges of the first Brillouin zone. The Bragg band gap for the P1 wave is the widest and contains the second Bragg band gap for the P2 wave. The first Bragg band gap for the P2 wave is too narrow to be observed from the real part of the wave number alone but still can be clearly identified from the imaginary part of the wave number. Overall, the complete Bragg band gap is small and covers the reduced frequency range $1495 < \Omega < 1547$ m/s.

Since the polarizations of the P1 and P2 waves share coupled longitudinal displacements, they can interfere whenever their dispersion curves cross. As a result of band anticrossing, two complete band gaps appear around $\Omega \sim 1000$ and 2000 m/s in Figs. 5(a) and 5(b). Vibration distributions at the marked points M1 and M2 near the first anticrossing region are presented in Fig. 5(d). Note that the polarizations of these Bloch waves change abruptly at the anticrossing, as can be attributed to level repulsion or avoided-crossing of the bands [53,54]. A pair of evanescent Bloch waves appear inside the anticrossing band gaps, connecting the extremal points of the two dispersion bands. The attenuation of the P1 and P2 waves are identical inside these band gaps, implying that the band gaps are complete.

In addition, the FRF curves of a finite metamaterial are calculated and presented in Fig. 5(c) for either 8 or 50 periods. Many oscillations come up in the FRF curves, even inside band gaps. These oscillations are caused by the excitation of Fabry–Pérot resonances of the finite structure. Since the polarization of the P1 and P2 waves share coupled longitudinal displacements, the resonances affect both waves simultaneously. Bragg band gaps cannot be clearly observed when only eight periods are considered. For 50 periods, the first P2 Bragg band gap is still missing in the FRF curves, because the imaginary

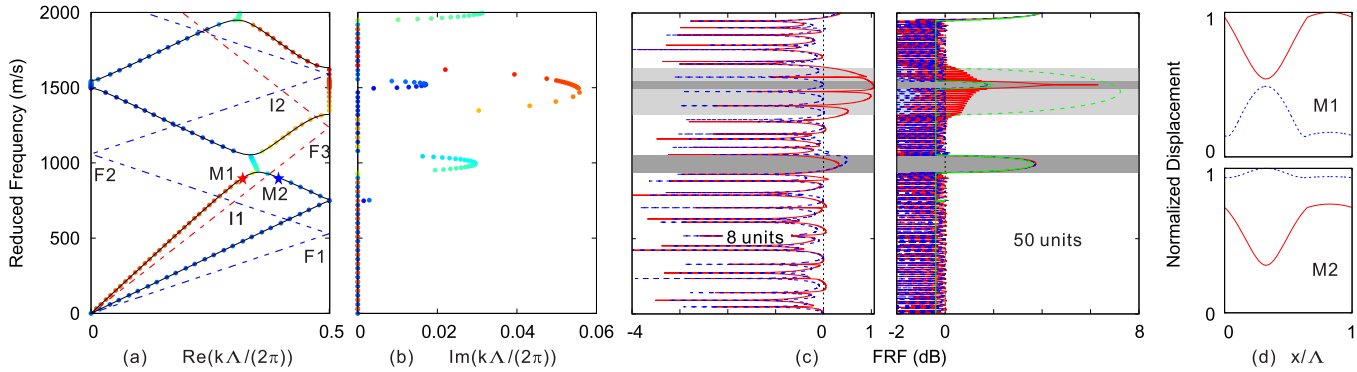

FIG. 5. Complex band structures for 1D lossless FSPM with periodic layers of FSP medium. Panels (a) and (b) illustrate the variation of the reduced frequency with the real and imaginary part of the wave vector, respectively. The solid lines represent the real band structures obtained by using Eqs. (13) and (15). The blue and red dashed lines are the dispersion curves of P1 and P2 waves for lossless FSP media, as obtained by Eq. (17). The color scale is the same as that in Fig. 2. FRF curves of a finite metamaterial with 8 or 50 unit cells are shown in panel (c). The solid and dashed lines represent the results for the excitation of P1 and P2 waves, respectively. The light gray region indicates the Bragg band gap for P1 wave in panel (a), while the gray regions show the complete band gaps for both P1 and P2 waves. The green lines represent the results predicted by using Eq. (19) through the imaginary part of the wave vector for P1 wave (dashed lines for P2 wave). Normalized displacement distributions at the marked points in panel (a) are illustrated in panel (d). The relative energy ratio is 0.74 at point M1 and 0.27 at point M2.

part of the wave number remains very small. The Bragg band gap for the P1 wave is corrupted by Fabry–Pérot resonances of the P2 wave. Interestingly, the anticrossing band gaps show the same attenuation for P1 and P2 waves, in agreement with the complex band structure. The approximation of the FRF curves inside band gaps as obtained with Eq. (19) are added with a green line to Fig. 5(c). They are in excellent agreement with FEM results in all complete band gaps. Inside the Bragg band gap for the P1 wave, the approximation breaks when wave P2 is not itself inside a band gap. Again, this is attributed to the coupling of longitudinal waves in the solid skeleton and in fluid saturated pores.

C. Effects of fluid viscosity

Next, we consider FSP metamaterials with varying viscosity, as shown in Fig. 6. Even when only a slight viscosity is added ($\eta = 10^{-7}$ Pa s), the dispersion curves are affected compared with the lossless case of the previous section. Regarding the real part of the wave number, the sharp corners at the edge of the Brillouin zone for the P1 wave become rounded. The degeneration of the evanescent modes at the anticrossings is now lifted for the imaginary part of the wave number. The P2 wave presents a larger attenuation than the P1 wave, in correspondence to the larger attenuation of the P2 wave in a homogeneous FSP medium shown in Fig. 3. FRF curves are also affected by viscosity. The Fabry–Pérot oscillations of the lossless system are washed out, especially inside the Bragg band gap for the P1 wave. The attenuation is generally larger for all frequencies and adds to the attenuation already present inside the band gaps.

When $\eta = 10^{-4}$ Pa s, f_c is beyond the frequency range considered and the attenuation of the P2 wave is expected to be quite large following Fig. 3. Thus, the dispersion relation of the P2 wave resembles that of the homogeneous FSP medium in Fig. 2. The anticrossings disappear from the FRF, because the P2 wave is too strongly attenuated to interfere with the P1

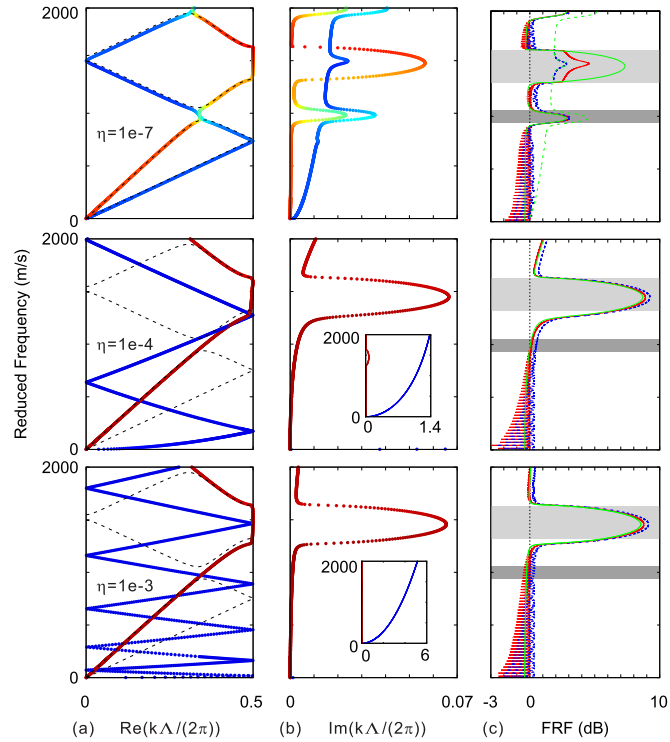

FIG. 6. Influence of fluid viscosity on complex band structures for 1D FSP metamaterials. Panels (a) and (b) show the variation of the reduced frequency with the real and imaginary part of the reduced wave number. The color scale is the same as that in Fig. 2. The insets in (b) show a larger view of the imaginary part of the wave number. The attenuation properties of a finite metamaterial with 50 periods are shown in panel (c). The red solid and blue dashed lines represent the results for the excitation of u_x and w_x, respectively. The green lines represent the results predicted by Eq. (19) for the P1 wave (green dashed lines for the P2 wave). The gray areas indicate the band gaps for the lossless FSPM in Fig. 5.

wave. The Bragg band gaps for the P2 wave also disappear. When the viscosity is further increased to $\eta = 10^{-3}$ Pa s, the same observations amplify. Interestingly, the base attenuation for the P1 wave (outside the Bragg band gap) is smaller than for $\eta = 10^{-4}$ Pa s. This observation is in correspondence with the decrease of the attenuation of the P1 wave in Fig. 3(b) for larger viscosities. With an increase in viscosity, the number of foldings for the P2 wave generally increases, but the same number for the P2 wave is almost unchanged. This could also be explained by the distinct variation of phase velocity of the P2 wave with a change in viscosity indicated by Fig. 3(a). For both excitations, the FRF curves have only small differences at large viscosity. Generally, the transmission of the P1 wave dominates the frequency response. As a result, the FRF curves can be closely approximated by considering only the least evanescent P1 wave.

It is also noted that the curvature of the lower round corner of the Bragg band gap for P1 wave first increases and then decreases. This can be simply explained by expanding $\omega(k)$ in powers of complex k about the zone edge $k_0 = \pi/d$ via a Taylor expansion [55], i.e.,

$$\Delta\omega = \omega(k) - \omega(k_0) \approx \zeta \mathrm{Re}((\Delta k)^2) = \zeta(g^2 - h^2), \quad (24)$$

where ζ is a constant related to the second derivative of the band, and $\Delta k = g + ih$. For the same $\Delta\omega > 0$ and a different viscosity, since the attenuation in Fig. 3(b) first increases and then decreases, the corresponding imaginary part first increases then decreases. Then h follows a similar variation, and so does g according to Eq. (24). Hence, the corners first get rounded and then become sharper.

D. Effects of fluid porosity

Porosity is also an important factor for FSP media. In this section, we consider the influence of fluid porosity on the complex band structures and the attenuation spectra. For comparison, we also consider the system with zero porosity. In this case, the system reduces to a 1D elastic layered metamaterial, the band structure of which is plotted with a dashed line in Fig. 7; no P2 wave exists in this case. Even when a small porosity ($\phi = 0.05$) is considered, the P2 wave comes up and the phase velocity of the P1 wave decreases. Correspondingly, the Bragg band gap for the P1 wave shifts downward. Comparing with Fig. 4, with an increase in porosity, the phase velocity of the P2 wave increases monotonically and there are less foldings in the real part of the P2 wave. In contrast, the phase velocity of the P1 wave first decreases and then increases, but the relative changes remain small. The real parts for $\phi = 0.24$ and 0.45 are thus similar. Both outside and inside the Bragg band gap, the imaginary wave number of the P1 wave increases monotonically with porosity, leading to an overall lower transmission. This observation is in contrast with the variations of attenuation for the P1 wave in a homogeneous FSP medium shown in Fig. 4(b). We attribute this difference to the periodicity of the FSPM. It is also noted that the upper (lower) corner of the band gap generally becomes more rounded (sharper) with an increase in the fluid porosity. This variation is explained by Eq. (24) as in the case of viscosity.

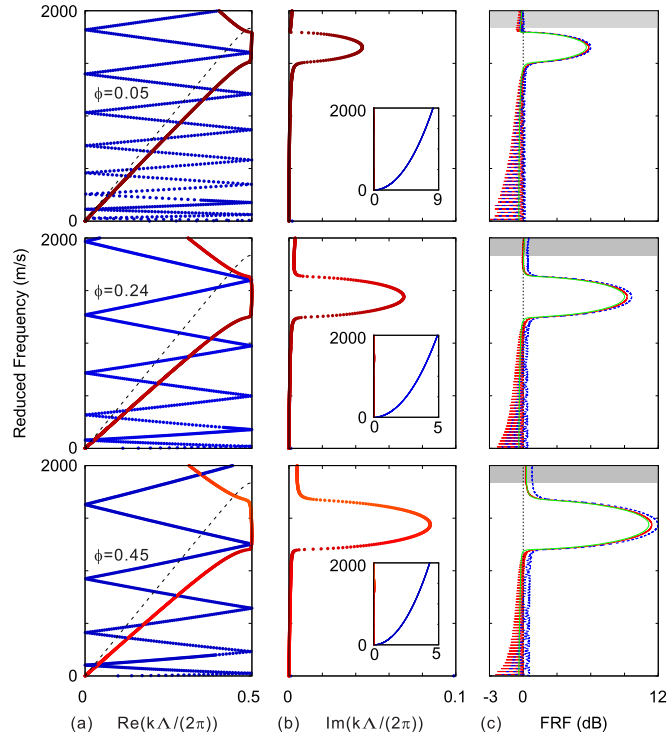

FIG. 7. Influence of porosity on the complex band structures for 1D FSPMs. Panels (a) and (b) show the variation of the reduced frequency with the real and imaginary parts of the reduced wave number. The dashed lines are the dispersion curves for $\phi = 0$. The color scale is the same as that in Fig. 2. FRF curves for a finite metamaterial with 50 periods are shown in panel (c). The red solid and blue dashed lines represent the results for the excitation of u_x and w_x, respectively. The green lines present the results of Eq. (19) for the P1 wave.

V. CONCLUSIONS

This paper has presented a comprehensive analysis of wave propagation in 1D fluid-saturated porous metamaterials (FSPMs) described by Biot's model and supporting two longitudinal waves, P1 and P2. Complex band structures and harmonic responses of 1D FSPMs were calculated by a finite element method. A theoretical analysis of longitudinal wave motion in homogeneous FSP media was conducted. Numerical results match perfectly analytical ones for homogeneous FSP media. It is found that the material parameters of the pore fluid have a strong influence on both complex band structures and FRF curves. With an increase (decrease) in viscosity (porosity), the attenuation in the passing bands is first enhanced and then reduced. Inside Bragg band gaps, the attenuation varies in the opposite way. Anticrossing band gaps can be generated by level repulsion between the fast P1 wave and the slow P2 wave when viscosity is negligible. These anticrossing band gaps soon disappear, however, as viscosity increases. With an increase in fluid porosity, attenuation increases monotonically inside passing bands and Bragg band gaps.

Generally speaking, the P2 wave is highly attenuated and influenced by material parameters. The P1 wave then plays the key role in the transmission though a finite periodic structure. In the limit that the influence of the P2 wave has been removed

by viscosity, the frequency response is well predicted by considering only the least evanescent P1 wave.

The present work is limited to 1D periodic metamaterials and should be extended to the two-dimensional (2D) and three-dimensional (3D) cases. In this case, appropriate independent variables should be chosen, because there are six displacements but only four degrees of freedom [41]. The influence of other complex interface conditions on wave propagation in FSPMs should be discussed [56]. The case of surface waves [57,58] propagating over a fluid-saturated porous metamaterial is also of interest. These different problems are significant for the development of novel metamaterials applied to the mitigation of blast and/or seismic waves.

ACKNOWLEDGMENTS

Financial support by the National Natural Science Foundation of China (11702017 and 11532001) is gratefully acknowledged. V.L. acknowledges financial support by the EIPHI Graduate School (ANR-17-EURE-0002). Y.-F.W. also acknowledges financial support from Young Elite Scientists Sponsorship Program by CAST (No. YESS20170022).

[1] S. Prakash, *Soil Dynamics* (McGraw-Hill, New York, 1981).
[2] A. Jain and D. K. Soni, in *Proceedings of 3rd WSEAS International Conference on Applied and Theoretical Mechanics* (WSEAS Press, Puerto De La Cruz, Spain, 2007), Vol. 3, p. 163.
[3] K. A. Kuo and H. E. M. Hunt, Appl. Mech. Rev. **65**, 031003 (2013).
[4] A. Niousha and M. Motosaka, WIT Transactions on The Built Environment **57**, 191 (2001).
[5] M. S. Kushwaha, P. Halevi, L. Dobrzyński, and B. Djafari-Rouhani, Phys. Rev. Lett. **71**, 2022 (1993).
[6] M. I. Hussein, M. J. Leamy, and M. Ruzzene, Appl. Mech. Rev. **66**, 040802 (2014).
[7] Z. Liu, X. Zhang, Y. Mao, Y. Y. Zhu, Z. Yang, C. T. Chan, and P. Sheng, Science **289**, 1734 (2000).
[8] Z. Liu, C. T. Chan, and P. Sheng, Phys. Rev. B **71**, 014103 (2005).
[9] G. Ma and P. Sheng, Sci. Adv. **2**, e1501595 (2016).
[10] M. S. Kushwaha and P. Halevi, Appl. Phys. Lett. **64**, 1085 (1994).
[11] G. F. Jia and Z. F. Shi, Earthq. Eng. Eng. Vib. **9**, 75 (2010).
[12] A. Malcolm and D. P. Nicholls, J. Acoust. Soc. Am. **129**, 1783 (2011).
[13] J. Bao, Z. F. Shi, and H. J. Xiao, J. Eng. Mech. **138**, 761 (2012).
[14] S. H. Kim and M. P. Das, Mod. Phys. Lett. B **26**, 1250105 (2012).
[15] Z. F. Shi and J. K. Huang, Soil Dyn. Earthq. Eng. **50**, 204 (2013).
[16] S. J. Mitchell, A. Pandolfi, and M. Ortiz, J. Mech. Phys. Solids **65**, 69 (2014).
[17] A. Colombi, P. Roux, S. Guenneau, P. Gueguen, and R. V. Craster, Sci. Rep. **6**, 19238 (2016).
[18] D. J. Colquitt, A. Colombi, R. V. Craster, P. Roux, and S. R. L. Guenneau, J. Mech. Phys. Solids **99**, 379 (2017).
[19] S. Brûlé, E. H. Javelaud, S. Enoch, and S. Guenneau, Phys. Rev. Lett. **112**, 133901 (2014).
[20] Y. Yan, A. Laskar, Z. Cheng, F. Meng, Y. Tang, Y. L. Mo, and Z. F. Shi, J. Appl. Phys. **116**, 044908 (2014).
[21] A. Colombi, D. Colquitt, P. Roux, S. Guenneau, and R. V. Craster, Sci. Rep. **6**, 27717 (2016).
[22] H. Franklin, F. Luppé, and J. M. Conoir, J. Acoust. Soc. Am. **135**, 2513 (2014).
[23] T. Weisser, J.-P. Groby, O. Dazel, F. Gaultier, E. Deckers, S. Futatsugi, and L. Monteiro, J. Acoust. Soc. Am. **139**, 617 (2016).
[24] A. Alevizaki, R. Sainidou, P. Rembert, B. Morvan, and N. Stefanou, Phys. Rev. B **94**, 174306 (2016).
[25] A. Alevizaki, R. Sainidou, P. Rembert, B. Morvan, and N. Stefanou, Phys. Rev. B **95**, 214306 (2017).
[26] W. Trabelsi, H. Franklin, A. Tinel, and S. Derible, Ultrasonics **54**, 1097 (2014).
[27] H. Deresiewicz, Bull. Seismol. Soc. Am. **52**, 627 (1962).
[28] R. D. Stoll and G. M. Bryan, J. Acoust. Soc. Am. **47**, 1440 (1970).
[29] B. R. Simon, O. C. Zienkiewicz, and D. K. Paul, Int. J. Numer. Anal. Methods Geomech. **8**, 381 (1984).
[30] A. Nur, *Wave Propagation in the Two-Phase Media* (Petroleum Industry Press, Beijing, 1986).
[31] M. A. Biot, J. Acoust. Soc. Am. **28**, 168 (1956).
[32] M. A. Biot, J. Acoust. Soc. Am. **28**, 179 (1956).
[33] T. J. Plona, Appl. Phys. Lett. **36**, 259 (1980).
[34] N. C. Dutta, Appl. Phys. Lett. **37**, 898 (1980).
[35] J. M. Carcione, J. Acoust. Soc. Am. **99**, 2655 (1996).
[36] Y. S. Wang and Z. M. Zhang, J. Acoust. Soc. Am. **103**, 695 (1998).
[37] L. De Ryck, J. P. Groby, P. Leclaire, W. Lauriks, A. Wirgin, Z. E. A. Fellah, and C. Depollier, Appl. Phys. Lett. **90**, 181901 (2007).
[38] Y. Liu and L. T. Gao, Int. J. Solids Struct. **45**, 4860 (2008).
[39] A. Pooladi, M. Rahimian, and R. Y. S. Pak, Appl. Math. Model. **50**, 177 (2017).
[40] Y. Liu, K. Liu, L. T. Gao, and T. X. Yu, J. Sound Vib. **282**, 863 (2005).
[41] M. N. Kazi-Aoual, G. Bonnet, and P. Jouanna, J. Acoust. Soc. Am. **84**, 1883 (1988).
[42] D. L. Johnson, J. Koplik, and R. Dashen, J. Fluid Mech. **176**, 379 (1987).
[43] P. N. J. Rasolofosaon, Appl. Phys. Lett. **52**, 780 (1988).
[44] D. L. Johnson, T. J. Plona, and H. Kojima, J. Appl. Phys. **76**, 115 (1994).
[45] J. Allard and N. Atalla, *Propagation of Sound in Porous Media: Modelling Sound Absorbing Materials*, 2nd ed. (John Wiley & Sons, United Kingdom, 2009).
[46] Y.-F. Wang, Y.-S. Wang, and V. Laude, Phys. Rev. B **92**, 104110 (2015).
[47] V. Laude, Y. Achaoui, S. Benchabane, and A. Khelif, Phys. Rev. B **80**, 092301 (2009).
[48] J. S. Jensen, J. Sound Vib. **266**, 1053 (2003).
[49] V. Romero-García, J. V. Sánchez-Pérez, S. Castiñeira-Ibáñez, and L. M. Garcia-Raffi, Appl. Phys. Lett. **96**, 124102 (2010).

[50] V. Laude, *Phononic Crystals: Artificial Crystals for Sonic, Acoustic, and Elastic Waves* (Walter de Gruyter GmbH, Berlin, 2015).
[51] D. L. Johnson, T. J. Plona, C. Scala, F. Pasierb, and H. Kojima, Phys. Rev. Lett. **49**, 1840 (1982).
[52] D. P. Schmitt, J. Acoust. Soc. Am. **86**, 2397 (1989).
[53] D. L. Johnson and T. J. Plona, J. Acoust. Soc. Am. **72**, 556 (1982).
[54] T.-T. Wu and Z.-G. Huang, Phys. Rev. B **70**, 214304 (2004).
[55] J. D. Joannopoulos, S. G. Johnson, J. N. Winn, and R. D. Meade, *Photonic Crystals: Modeling the Flow of Light*, 2nd ed. (Princeton University Press, New Jersey, 2008).
[56] H. Deresiewicz and R. Skalak, Bull. Seismol. Soc. Am. **53**, 783 (1963).
[57] K. Ahn, Y. A. Kosevich, and M. W. Kim, Europhys. Lett. **60**, 241 (2002).
[58] Y. A. Kosevich, K. Ahn, and M. W. Kim, Phys. Rev. Lett. **90**, 059601 (2003).